Full Paper

Propellants, Explosives, Pyrotechnics

DOI: 10.1002/prep.202000221

On the Pressure Generated by Thermite Reactions Using Stress-Altered Aluminum Particles

Alan Williams,*[a] Islam Shancita,*[a] Igor Altman,*[b] Nobumichi Tamura,*[c] and Michelle L. Pantoya*[a]

Abstract: This study examines pressure build-up and decay in thermites upon impact ignition and interprets reactivity based on the holistic pressure history. The thermite is a mixture of aluminum (Al) combined with bismuth trioxide (Bi_2O_3) powder. Four different Al particles sizes were examined that ranged from 100 nm to 18.5 μm mean diameter and for each size, two different Al powder treatments were examined: stress-altered compared to untreated, as-received Al powder. Stress-altered Al powders have been shown to be more reactive, such that the stress-altered Al powder thermites offer a metric for analyzing thermite reactivity in terms of pressure development compared to untreated Al powder. In a binary thermite system, multiple phase changes and interface chemistry influence the transient pressure response during reaction. Results reveal three key pressure metrics that need consideration specifically for thermite combustion: (1) delay time to peak pressure, (2) peak pressure, and (3) decay after peak pressure. Our experiments show that a lower peak pressure corresponds with higher thermite reactivity because aluminum consumption of oxygen generated by decomposing solid oxidizer reduces the peak pressure. Faster rates of reaction consume oxygen at higher rates such that pressure development becomes more limited than less reactive thermites and the result is a lower peak pressure. This conclusion is opposite of traditional studies using metal fuels with a gaseous environment that typically show higher peak pressures correspond with greater reactivity.

Keywords: Pressure · Thermite · Stress-Altered Powders · Aluminum · Solid Fuels · Pressurization Rate · Metal Oxides

1 Introduction

■■ dear author, please provide Corresponding author, thank you ■■

■■Dear Author, please provide journal abbreviation, if possible. According to the Author's Guidelines (Wiley) the References should be structured as follows: **Example for Journals**: A. Autor, B. R. Coauthor, Title of the article, *Z. Anorg. Allg. Chem.* **2006**, *632*, 1–5 **Example for Books**: a) P. Zuman, *The Elucidation of Organic Electrode Processes*, Academic Press, New York **1969**, p. 170; b) H. M. Sutton, Flow Properties of Powders and the Role of Surface Character, in: *Characterization of Powder Surfaces* (Eds.: G. D. Parfitt, K. S. Sing), Academic Press, London **1976**, p. 107.
Example for others: ***see*** http://onlinelibrary.wiley.com/journal/10.1002/(ISSN)1521-4087/homepage/2014_guide.html
■■

When metal fuel particles, such as aluminum (Al), burn in a gaseous environment, the traditional approach to describing explosive reactivity from the pressure history data is to quantify the peak pressure and pressurization rate within the chamber after reaction initiation [1]. The peak pressure is the maximum pressure achieved during the transient event and characterizes the overall energy released by combustion. Correspondingly, the magnitude for the peak pressure rise is on the order of 10, considering a variation in temperature from ambient (300 K) to the characteristic adiabatic flame temperature (3000 K) and assuming the ideal gas law [2,3]. The pressurization rate describes the reaction rate and is often presented in terms of the deflagration index which includes the chamber volume [1]. These two metrics have been used to compare reactivity of different metal fuel particles in dust combustion studies in the obvious way: a higher peak pressure and pressurization rate corresponds to higher reactivity [4].

The applicability of peak pressure and pressurization rate metrics towards characterizing reactivity of thermite

[a] *A. Williams, I. Shancita, M. L. Pantoya*
Department of Mechanical Engineering, Texas Tech University, Lubbock, TX 79409, USA
**e-mail: alan.williams@ttu.edu*
shancita.islam@ttu.edu
michelle.pantoya@ttu.edu
[b] *I. Altman*
Combustion Sciences and Propulsion Research Branch, Naval Air Warfare Center Weapons Division, 1 Administration Circle, China Lake, CA 93555, USA
**e-mail: igor.altman@navy.mil*
[c] *N. Tamura*
Advanced Light Source, Lawrence Berkeley National Laboratory, Berkeley, CA 94720, USA
**e-mail: ntamura@lbl.gov*

Supporting information for this article is available on the WWW under https://doi.org/10.1002/prep.202000221

systems needs more in-depth consideration. At first glance, these metrics should also be applicable to thermites. However, a more complex reaction mechanism owing to the inclusion of a solid oxidizer and its interaction with the fuel particles, and, therefore, the way pressure evolves during reaction, may invalidate these seemingly straightforward metrics. The current paper is a first step to progressing the understanding of thermite reactivity and pressure achieved in the reacting thermite system.

Thermite reactions will be defined here by a reaction between a metal fuel, such as Al, and a metal oxide. The global thermite reaction can be described by Reaction (1).

$$(2y/3)Al + M_xO_y \rightarrow (y/3)Al_2O_3 + xM \quad (1)$$

In Rn. (1), M_xO_y is the metal (M) and oxide (O) with M valence 2y/x. The complication arises in resolving transient pressure in thermite systems because various condensed phase intermediates and end products, such as oxides, suboxides and alloys are formed throughout reaction and affect pressure progression. For example, Wang et al. [5] examined nanoparticle mixtures of Al and Bi_2O_3 and showed multiple pressure rises and decays throughout the duration of reaction due to the multiphase nature of the combustion process.

The transient pressure profiles generated by Wang et al. [5] for $Al + Bi_2O_3$ were further simulated by Martirosyan et al. [6]. Their simulation assumed all explosion energy was released into the gas phase instantaneously and used an explicit self-similar solution approach that was simplified without inclusion of condensed phase species evolution. Their results produced smooth pressure profiles with a single peak in pressure rise followed by continuous decay and their modeled peak pressure was a good estimate of the highest peak pressure measured experimentally.

Baijot et al. [7] further refined thermite pressure model development by including phase changes such as vapor and condensed phase reaction processes. The Baijot model [7] more accurately described the multiphase nature of the transient combustion process to resolve pressure variations that are influenced by melting, boiling, decomposition, and condensation processes. For the $Al + Bi_2O_3$ reaction, Baijot et al. [7] showed that peak temperature does not coincide with peak pressure and showed a succession of pressure peaks corresponding to the decomposition or evaporation onsets of various species. In particular, the initial pressure rise resulted from the decomposition of Bi_2O_3 into molecular oxygen and liquid bismuth that generated the initial pressure peak. The peak pressure was followed by evaporation of Bi which produced a gentle pressure shoulder alongside the initial peak pressure rise.

The above experimental and modeling studies on $Al + Bi_2O_3$ indicate that a completely different mechanism of pressure development is responsible for the peak pressure and pressurization rate in comparison to single fuel particle or dust combustion studies. For $Al + Bi_2O_3$ a major contribution to the pressure is created by the reaction by-products and succession of multi-phase decomposition and reaction processes. Therefore, in thermites it is not straightforward to relate a higher maximum peak pressure or pressurization rate to enhanced thermite reactivity.

This study qualitatively analyzes the mechanism of $Al + Bi_2O_3$ reaction by considering separate steps that are responsible for the pressure behavior during reaction. Our analysis is based on experiments performed for $Al + Bi_2O_3$ that are a function of the Al particle size ranging from nano-scale to micron-scale Al particle diameters. For each Al particle size two cases were examined: as-received Al particles that are described as untreated Al (UN–Al) and Al particles that were annealed at 300 °C for 15 minutes then quenched at a cooling rate of 11.14 °C/s to produce stress-altered Al particles identified as super-quenched Al (SQ–Al). Our previous research demonstrated SQ–Al particles exhibit enhanced reactivity compared to UN–Al, [8,9,10,11] and thus this stress-altered processing technique serves as a baseline for studying variations in reactivity when compared to UN–Al in the interpretation of the pressure measurements.

Comparing SQ–Al reactions to UN–Al reactions provides new insight on pressure evolution used to characterize reactive behavior, not only in the conventional peak pressure and pressurization rate sense, but also the influence of multi-phase reaction processes on pressure development from a holistic perspective. Stress-altered SQ–Al particles are at an elevated stress state and exhibit a unique feature of shell delamination from the core [10]. During annealing, Al powder is relieved of residual stresses and during fast quench, differences in thermal expansion coefficients between the Al core and Al_2O_3 shell develop a permanent stress at the core-shell interface. The shell becomes delaminated from the core and is theorized to fracture more easily. The core-shell delamination in SQ–Al is a function of Al particle size because μAl has shown 52% core-shell interfacial surface area delamination [9] while nAl has shown 81% core-shell interfacial surface area delamination [12]. Without support from the core, the shell more easily fractures thereby enhancing diffusion controlled reactions. Low-velocity impact testing of SQ Al was performed previously by Hill et al. [9] and showed that SQ $Al + Bi_2O_3$ achieved higher peak pressure compared to untreated $Al + Bi_2O_3$. An important distinction between Hill et al. [9] and this work is that they applied various magnitudes of impact energy for different treatments of Al to achieve the highest pressure possible. Here, comparing unique pressure histories from SQ–Al to UN–Al reactions provides a deeper understanding of the connections between pressure development and thermite reaction behavior.

2 Experimental

2.1 Aluminum Powders

Four aluminum (Al) powders that varied in average particle diameter were used and identified as: 100 nm (nAl) supplied from Novacentrix (Austin, TX), and three micron-scale Al (μAl) powders including: 1.5 μm supplied from Skyspring Nanopowder (Houston, TX), and 3 μm and 18.5 μm supplied from Sigma Aldrich (St. Louis, MO). Volume weighted size distributions for each powder were measured using a NiComp N3000 static particle size analyzer (Santa Barbara, CA) by dynamic light scattering (DLS) method. The size distributions were determined by suspending (3 mg) Al powder in (100 ml) of distilled water solution. The mixture was subjected to ultrasonic waves to break up agglomerates and ensure the particles were fully suspended within the distilled water using a Misonix Sonicator 3000. Particle size distributions are shown in *Supplementary Information*, Figure S1 with the measured mean diameter and standard deviation reported in Table 1 along with the label identifier for each powder. The annealing and quenching process does not alter the size distribution and this was confirmed previously for nAl powders in Bello et al [12] and μAl powders in McCollum et al [13].

2.2 Powder Annealing and Quenching Treatments

An Al powder annealing temperature of 300 °C held for 15 minutes was previously identified as effective, but the quenching rate applied to the annealed particles can significantly alter the microstructure of the core-shell particle [9]. The stress-altered Al particles studied here were annealed to the constant temperature of 300 °C for 15 minutes and quenched at a relatively fast cooling rate of 11.14 °C/s identified as 'super-quenched' (SQ–Al). This quenching rate deliberately induces delamination at the core-shell particle interface and has been shown to promote diffusion reactions [8].

Powder quenching was achieved using (250 mg) of Al powder loaded into a sealed, steel chamber that is well described by Hill et al. [9]. A thermocouple monitored the transient powder temperature during annealing and quenching using LabVIEW and National Instruments (NI) data acquisition hardware. Heating at a rate of 10 °C/min to 300 °C was achieved in a Vulcan multi-stage programmable furnace. The chamber was held at the annealing temperature of 300 °C for 15 minutes then removed and submerged in a quenching fluid composed of water, Dawn dish soap, simple green cleaner and sodium chloride described in detail previously [9]. The cooling rate was monitored by the thermocouple and is 11.14 °C/s.

Table 1. Particle size distributions including mean diameter and standard deviation.

Particle size	Mean diameter	Standard deviation
100 nm	96.7 nm	±11.8 nm
1.5 μm	1.6 μm	±0.27 μm
3 μm	3.1 μm	±0.5 μm
18.5 μm	18.6 μm	±3.2 μm

2.3 Strain Measurement

The dilatational strain for each Al particle size was measured at the Synchrotron X-ray Diffraction (XRD) Advanced Light Source facility at Lawrence Berkeley National Laboratory on beamline 12.3.2 using a micron focused synchrotron X-ray beam. Measurements from this beamline that quantify dilatational strain have been reported previously [9,13,14,15,16,17]. In a similar procedure, glass slides were coated with various μAl powder samples. The powder samples were scanned under the X-ray beam (either polychromatic or monochromatic) while a diffraction pattern was collected at each step using a DECTRIS Pilatus 1 M detector. While the polychromatic (Laue) patterns provide the shear components of the strain, the measurement of energy of one indexed reflection provides the missing dilatational component. Data were processed using XMAS software and details of the experimental setup and synchrotron XRD capabilities are described elsewhere [18,19].

The dilatational strain for all nAl powders was also measured using Synchrotron XRD at the same facility. In contrast to above measurements on μAl powder, data on nAl particles were taken with a 10×2 μ 12 keV monochromatic beam because the size from the white beam focus (around 1 μm) was not sufficiently small to resolve the nAl particles. For the nAl particles, data were taken in powder diffraction pattern mode and dilatational strain was derived from the shifts in 2θ values of the powder rings with respect to their unstrained positions. Powder patterns were taken with the detector at an angle of 50° and distance of 18 cm from the powder sample. Similar to the μAl powders, data were processed using XMAS software.

2.4 Mixture Preparation

All Al powders were mixed with bismuth(III) oxide (Bi_2O_3) to an equivalence ratio of 1.3 (i.e., slightly fuel rich). The Bi_2O_3 powder was obtained from Sigma Aldrich and ranged from 90–210 nm spherical particle diameter. Mixtures of up to 1.5 grams were prepared by sonicating the fuel and oxidizer particles in a 120 ml sample cup using 90 ml of acetone as the carrier fluid. The Misonix Sonicator 3000 enables programmed processing cycles of 10 seconds on and off for 2 minutes and this process breaks up agglomerates while maintaining ambient temperatures during mixing. The mixture was poured into a Pyrex dish and dried in a

fume hood for 24 hours. The powder was reclaimed through a 325 mesh sieve to further break up soft agglomerates before further experimentation.

2.5 Pellet Assembly

A Parr pellet press punch and die assembly was used with shims to achieve a constant volume for each pellet. The inner diameter of the die was 6.4 mm and the pellet height was 0.80 mm. To prepare the pellet, the die and holder was filled with 185.8 mg of $Al + Bi_2O_3$ mixture. The pellets were pressed to 90% of its theoretical maximum density (90% TMD) with an actual density of 7.3 g/cm^3.

2.6 Impact Testing

The drop-weight impact tester is fully described in Hill et al. [9], but will be summarized here for completeness. The device consists of a pressure cell shown in Figure 1(a)–(c), along with the impact test frame that includes a carriage holding weights that fall along vertical guide rails onto the pressure cell in Figure 1(d). As the carriage falls, it strikes the steel pin shown on the right side of Figure 1(c) that impacts the sample. Adjusting either the weight or height of the carriage provides adjustment for the amount of energy delivered to the pressure cell. Although the weight of the carriage may vary by adding or removing constituent cylindrical weights, the weight from test to test is held constant for this purpose, for a total weight of 4.37 kg, including the weights and carriage. The height of the carriage is fixed at 63.2 cm for every test. The pellet itself has a volume of 25.5 mm^3 and the internal volume of the chamber is 55.3 mm^3, resulting in a pellet to chamber volume ratio of 0.461.

Pressure data were acquired using a PCB Piezotronics pressure transducer (model 101 A06) having a sensitivity of 1.45 mV/kPa. A PCB signal conditioner (model 480 C02) amplified the signal for data acquisition and a PicoScope 5000 series was programmed to collect data at 100 kHz. All experiments were performed in triplicate for repeatability. Raw data from each event was filtered using a low pass filter cutoff at 4 kHz for clear display and analysis.

3 Results and Discussion

3.1 Strain Measurements

Table 2 presents the strain measurements for the four Al particle sizes. In terms of particle size, nAl shows considerably higher strain than its larger sized counterparts that are essentially equivalent because the data fall within a degree of uncertainty given the wide distribution. The UN–Al particles show negligible dilatational strain for all particle sizes. In fact, the measured dilatational strain for UN–Al particles was too small for accurate resolution (i.e., $<10^{-7}$) from the Synchrotron XRD instrumentation.

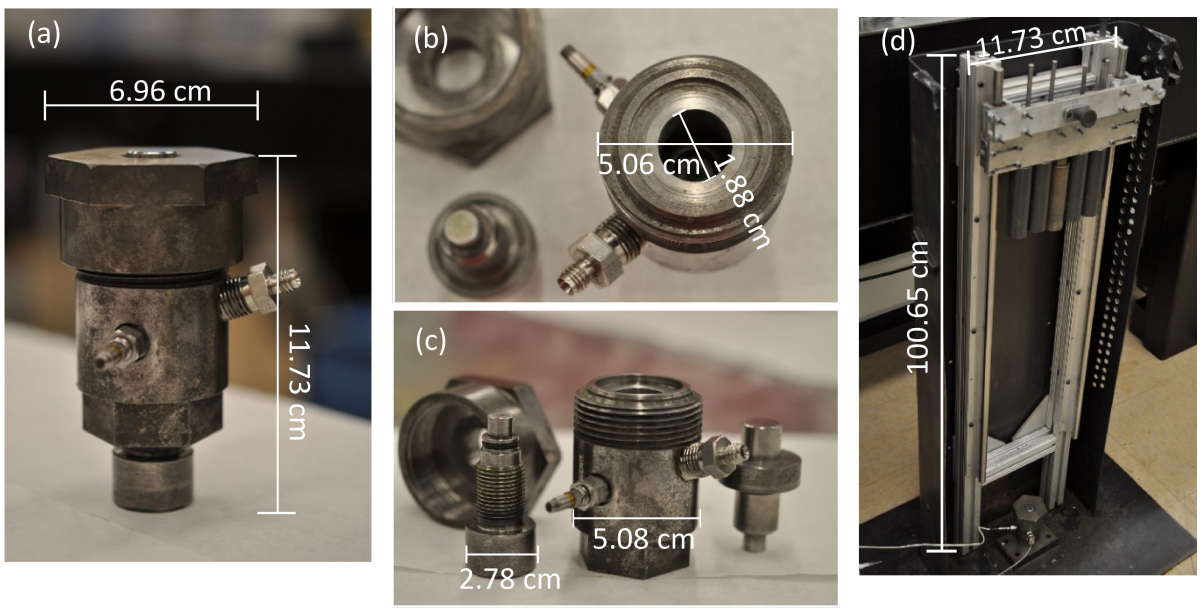

Figure 1. Drop-hammer impact test apparatus including (a) the assembled pressure cell, (b) the cell interior where the pellet is placed, as well as the pressure transducer and the optical fiber probe ports extruding from the cell, (c) the disassembled pressure chamber components, and (d) the completed setup where the weights of the carriage fall along the guide rails onto the cell.

Table 2. Synchrotron XRD strain measurements and standard deviation in measured values for SQ–Al particle sizes indicated.

Particle Size	Strain
100 nm	$40\times10^{-5}\pm15\times10^{-5}$
1.5 μm	$4\times10^{-5}\pm20\times10^{-5}$
3.0 μm	$3\times10^{-5}\pm26\times10^{-5}$
18.5 μm	$10\times10^{-5}\pm19\times10^{-5}$

3.2 Pressure Data

There are two main variables examined in this study: (1) the influence of stress-altered treatment on Al combustion and (2) the influence of Al particle size on combustion. The Bi_2O_3 particles remained the same throughout all testing as well as the stoichiometry and pellet bulk density.

Figure 2 shows the influence of stress-altering the Al particles on pressure profile for the $Al+Bi_2O_3$ reaction. The data focuses on the first ms of reaction but the same graphics extended to longer time scales are included in *Supplementary Information*. For each Al particle size, the SQ–Al thermite continuously produced a lower initial peak pressure followed by a similar decay. The delay time from start of reaction until peak pressure, considered to occur when pressure rises to 2% of the peak, is also shown in Table 3.

Table 3. Reaction delay times (t_d) in ms and peak pressure in MPa for UN–Al and SQ–Al thermite reactions with the standard deviation (σ) in measured values for each case.

Al Particle Size	t_d (ms) UN-Al $+Bi_2O_3$	σ (ms)	t_d (ms) SQ-Al $+Bi_2O_3$	σ (ms)	P (MPa) UN-Al $+Bi_2O_3$	σ (MPa)	P (MPa) SQ-Al $+Bi_2O_3$	σ (MPa)
100 nm	0.18	0.09	0.12	0.02	7.20	1.92	5.34	0.19
1.5 μm	0.14	0.04	0.17	0.05	7.05	0.39	6.72	0.56
3.0 μm	0.23	0.05	0.19	0.04	6.22	0.74	5.46	0.99
18.5 μm	0.16	0.06	0.14	0.03	5.73	0.45	3.69	0.78

Figure 3 further shows the pressure history for all thermites with UN–Al or SQ–Al particle sizes examined at the same 1.0 ms time scale as shown in Figure 2. Consistently, the 18.5 μm diameter Al particles exhibit the lowest pressure response throughout reaction and the 1.5 μm diameter

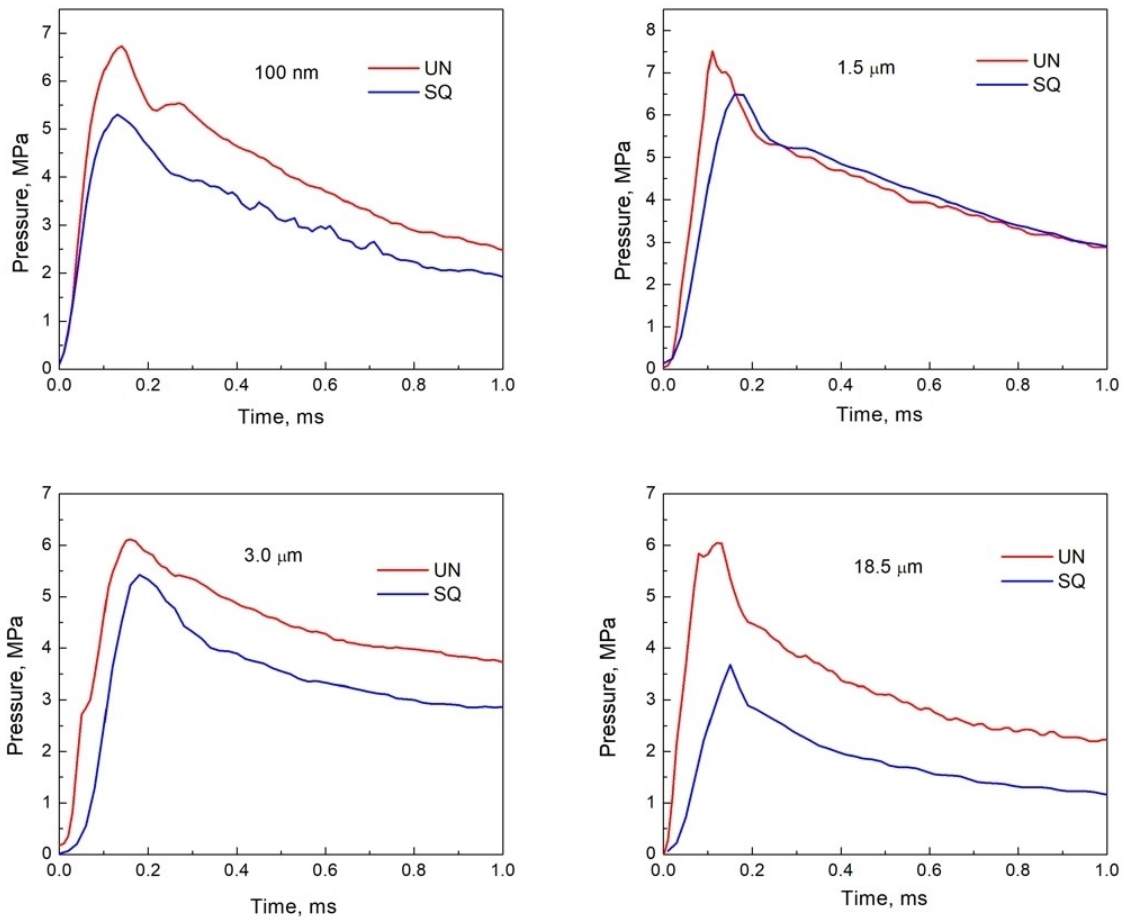

Figure 2. Pressure as a function of time for UN–Al (red curves) and SQ–Al (blue curves) mixtures of $Al+Bi_2O_3$ for various Al particle sizes indicated on the graphs.

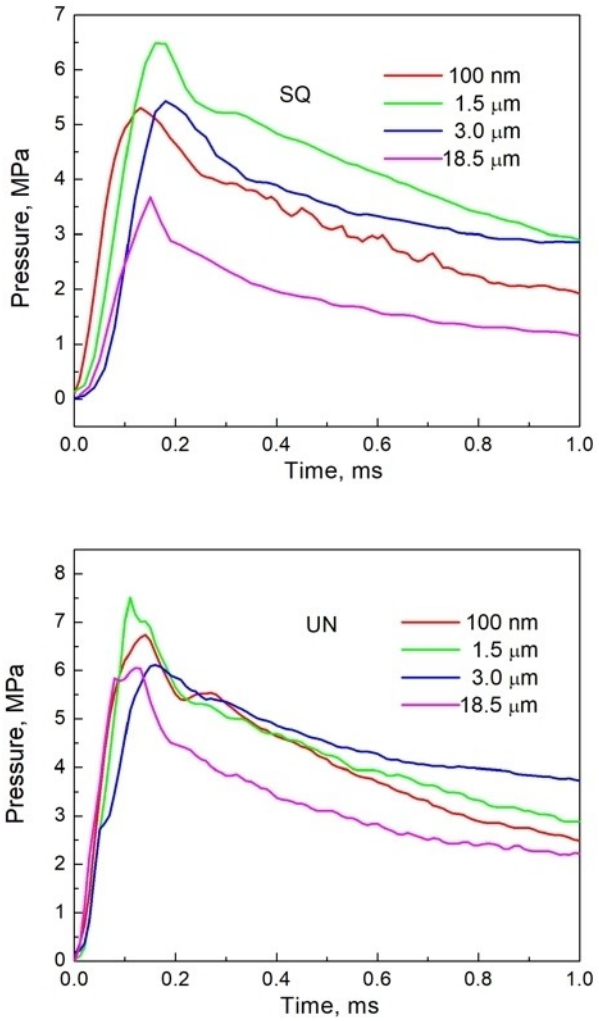

Figure 3. Pressure as a function of time for varied Al particle sizes in the Al + Bi_2O_3 reaction. The Al particle processing condition is indicated on the graphs (super-quenched Al, SQ and untreated Al, UN). Reactivity is a stronger function of particle size for SQ-Al + Bi_2O_3 than for UN-Al + Bi_2O_3.

Al particles exhibit the highest pressure response throughout reaction.

There are three major points seen in Figures 2 and 3: (1) the time delay between the reaction initiation and the peak pressure is nearly the same in all thermites studied; (2) the peak pressure value is constantly higher in the UN–Al thermites compared to the SQ–Al thermites; (3) the pressure decay after the peak is similar in all thermites. An analysis of these three components of the pressure history allows one to suggest the controlling mechanism for pressure build-up in thermites.

As it is well-known, the major contribution to pressure development during the thermite reaction resides with the decomposition of oxidizer (e.g., Bi_2O_3 in our system), and the measured pressure can be assumed to be caused by the oxygen pressure [7]. When considering oxygen from the environment, the O_2 concentration remains constant in the contained pressure cell across tests thus is assumed to be a negligible contribution for the differences in reactions observed. Then, besides the solid surface reaction that is responsible for initiation, oxidation of Al particles by the formed oxygen from the oxidizer is also possible. Oxygen consumption by Al leads to conversion of intermediate and product oxides that reduce pressure. When oxygen liberated from the oxidizer is consumed, a higher rate of combustion will coincide with a lower system pressure. As a result, the higher peak pressure will correspond to the material with the lowest metal-oxygen particle reactivity. For example, in the Al and Bi_2O_3 reaction, if oxygen is liberated in large quantities, pressure will increase; but, if the oxygen liberated is instantaneously consumed by reaction, a lower peak pressure indicates faster conversion of liberated oxygen to intermediate and product species. Therefore, the thermites containing SQ–Al exhibit lower peak pressure than UN–Al thermites such that SQ–Al demonstrates greater reactivity in the thermite (see Figure 2).

Not only do SQ–Al particles exhibit greater reactivity under impact ignition conditions [9], but SQ–Al particles have also been examined in dust combustion [11] and single particle combustion experiments [8]. Williams et al. [11] showed that SQ Al particles demonstrated higher combustibility in oxygen compared with UN–Al particles. Similarly, when Al particles were individually ignited by a CO_2 laser in an air environment, SQ–Al particles exhibited reduced ignition delay times and burn times compared with UN–Al [8]. Studies on SQ–Al combustion under impact ignition, dust cloud, and as single particles thermally ignited in an oxidizing gaseous environment all show SQ–Al facilitates diffusion oxidation reactions because delamination at the core-shell interface resulting from stress-altering the particles weakens the shell and promotes diffusion. Therefore, the SQ–Al thermite pressure response in Figure 2 indicates lower peak pressure corresponds to higher reactivity.

Figure 3 shows the variation in pressure evolution as a function of Al particle size. Under thermal or equilibrium reaction conditions, Al particle ignition and reaction are controlled by diffusion of fuel or oxygen through the shell. This is opposite in the impact ignition tests (Figure 2 and 3) that induce rupturing of the protective shell and direct exposure of the metal core to oxygen from the solid oxidizer. In impact ignition, the shell is not a pathway for the diffusion reaction mechanism. In the case of impact ignition, there are two process for reaction between the solid fuel and oxidizer particles. The first process is related to the reaction between Al and Bi_2O_3 particles, which leads to pressure increase due to oxygen liberation from Bi_2O_3. The second process is related to the reaction between the liberated oxygen and Al particles, which leads to the pressure decrease due to the oxygen consumption. Since the effects on pressure are opposite between these two processes, the resulting pressure appears to be relatively size independent

and a stronger function of aluminum particle treatment (i.e., stress altered versus untreated). However, using Figure 2 as a guide for key features signifying heightened reactivity, the largest SQ–Al particle size, 18.5 μm diameter, exhibits the lowest peak pressure (Figure 3) suggesting that the largest particles may be most influenced by stress altering because they exhibit the greatest reactivity in comparison to all other Al particle sizes. Both 3 μm and 100 nm Al particles exhibit similar pressure development and 1.5 μm Al has the highest peak pressure suggesting this size range may not benefit as significantly from stress altering. In fact, the peak pressure for 1.5 μm Al is nearly the same for UN–Al as for SQ–Al (Figure 3). For UN–Al the variation in Al particle size has little effect on thermite reaction under impact conditions as evidenced by similar peak pressure and overall pressure development (Figure 3).

The pressure decay after the peak needs separate attention. The pressure decay is due to the oxygen consumption in aluminum combustion. The decay rate is expected to be dependent on the Al particle burn rate, and, therefore, on the Al particle size. However, in the consolidated thermite, Al particles cannot be considered as individually burning. Indeed, as soon as the system temperature reaches the Al melting point upon impact: Al melts, Al_2O_3 shells fracture, and instead of individual metal particles, molten Al coalesces and a film is formed from molten metal that will burn. The burn rate of that film, and, correspondingly, the rate of the pressure drop does not depend on the original Al particle size. In fact, the pressure decay seen in Figures 2 and 3 is not a function of particle size and consistent with the theory of Al melting followed by metal film formation. The formed metal film wets Bi_2O_3 particles, which prevent further oxygen release from the solid oxidizer, and, therefore, stops the pressure rise. Then, surface wetting may be responsible for variations in pressure peak, i.e., the pressure peak occurs at the moment of nearly complete wetting. This film melting and oxidizer wetting mechanism may explain an unforeseen observation that the peak pressure occurs at about the same time delay after reaction initiation regardless of Al particle size. Indeed, if wetting is responsible for the stoppage of pressure build-up, then the wetting time rather than the reaction rate is the major factor determining the time delay. The wetting time depends neither on the Al particle stress-dependent reactivity nor on Al particle size, which explains a nearly exact delay time (Table 3) in all our experiments. Based on these observations (Figures 2 and 3), processes at the interface of particles such as wetting should be considered in developing a detailed thermite reaction model.

4 Conclusions

Pressure development in a consolidated thermite under impact ignition conditions cannot be interpreted by the same metrics as Al powder combustion. Our experiments show that a lower peak pressure corresponds with higher thermite reactivity because consumption of oxygen upon aluminum reaction reduces the peak pressure. Faster rates of reaction consume oxygen at higher rates such that pressure development becomes more limited than less reactive thermites and the result is a lower peak pressure. Generally, the pressure histories show nearly the same response for as-received, untreated Al powder thermites regardless of Al particle size indicating burning rate is independent of particle size for the Al size range investigated. Under impact ignition, the consolidated powders melt and flow into a film as opposed to individual particle burning. The molten film may wet the surrounding solid oxidizer, thereby limiting oxygen release. This mechanism is consistent with all results for all thermites investigated that show similar delay times to peak pressure and pressure decay behavior. Overall, this study shows the multiphase processes at the interface of particles effects their reactivity and should be considered when developing thermite combustion models.

Acknowledgements

The authors are grateful for support from Office of Naval Research under ONR contract N00014-16-1-2079 and our program manager, Dr. Chad Stoltz. Also, I.A. is thankful for funding from the NAVAIR ILIR program managed at the ONR and administered by Dr. Alan Van Nevel. The Synchrotron XRD used beamline 12.3.2, a resource at the Advanced Light Source, supported by the Director, Office 439 of Science, Office of Basic Energy Sciences, Materials Science Division, of the U.S. 440 Department of Energy under Contract No. DE-AC02-05CH11231 at LBNL.

Data Availability Statement

The data that support the findings of this study are available from the corresponding author upon reasonable request.

References

[1] R. Lomba, S. Bernard, P. Gillard, C. Mounaïm-Rousselle, F. Halter, C. Chauveau, T. Tahtouh and O. Guézet, "Comparison of Combustion Characteristics of Magnesium and Aluminum Powders," *Combustion Science and Technology*, *vol. 188*, 11–12, pp. 1857–1877, **2016**.

[2] P. R. Santhanam, V. K. Hoffmann, M. A. Trunov, E. L. Dreizin, "Characteristics of Aluminum Combustion Obtained from Constant-Volume Explosion Experiments," *Combustion Science and Technology*, *vol. 182*, no. 7, pp. 904–921, **2010**.

[3] K. L. Cashdollar and I. A. Zlochower, "Explosion temperatures and pressures of metals and other elemental dust clouds," *Journal of Loss Prevention in the Process Industries*, *vol. 20*, no. 4–6, pp. 337–348, **2007**.

[4] M. Silvestrini, B. Genova, F. J. L. Trujillo, "Correlations for flame speed and explosion overpressure of dust clouds inside in-

dustrial enclosures," *Journal of Loss Prevention in the Process Industries*, *vol. 21*, no. 4, pp. 374–392, **2008**.

[5] L. Wang, D. Luss, K. S. Martirosyan, "The behavior of nano-thermite reaction based on Bi2O3/Al," *Journal of Applied Physics*, *vol. 110*, no. 7, pp. 074311, **2011**.

[6] K. S. Martirosyan, M. Zyskin, C. M. Jenkins and Y. Horie, "Modeling and simulation of pressure waves generated by nano-thermite reactions," *Journal of Applied Physics*, *vol. 112*, no. 9, pp. 094319, **2012**.

[7] V. Baijot, L. Glavier, J.-M. Ducéré, M. D. Rouhani, C. Rossi, A. Estève, "Modeling the Pressure Generation in Aluminum-Based Thermites," *Propellants*, *Explosives*, *Pyrotechnics*, *vol. 40*, no. 3, pp. 402–412, **2015**.

[8] K. Hill, M. L. Pantoya, E. Washburn, J. Kalman, "Single particle combustion of pre-stressed aluminum," *Materials*, *vol. 12*, no. 11, pp. 1–6, **2019**.

[9] K. J. Hill, N. Tamura, V. I. Levitas and M. L. Pantoya, "Impact ignition and combustion of micron-scale aluminum particles pre-stressed with different quenching rates," *Journal of Applied Physics*, *vol. 124*, no. 11. pp. 115903, **2018**.

[10] K. J. Hill, J. Warzywoda, M. L. Pantoya, V. I. Levitas, "Dropping the hammer: Examining impact ignition and combustion using pre-stressed aluminum powder," *J. Appl. Phys.*, *vol. 122*, no. 12, pp. 125102, **2017**.

[11] A. Williams, I. Shancita, N. G. Vaz, T. Tran-Ngo, A. Demko, I. Altman, K. J. Hill, D. Tunega, A. J. A. Aquino, M. L. Pantoya, "Stress-altered aluminum powder dust combustion," *Journal of Applied Physics*, *vol. 127*, no. 17, pp. 175110, **2020**.

[12] M. N. Bello, A. M. Williams, V. I. Levitas, N. Tamura, D. K. Unruh, J. Warzywoda, M. L. Pantoya, "Highly reactive energetic films by pre-stressing nano-aluminum particles," *RSC Advances*, *vol. 9*, no. 69, pp. 40607–40617, **2019**.

[13] J. McCollum, M. L. Pantoya, N. Tamura, "Improving aluminum particle reactivity by annealing and quenching treatments: Synchrotron X-ray analysis of strain," *Acta Materialia*, *vol. 106*, pp. 495–501, **2016**.

[14] V. I. Levitas, J. McCollum, M. Pantoya, "Pre-Stressing Micron-Scale Aluminum Core-Shell Particles to Improve Reactivity," *Scientific Reports*, *vol. 5*, no. 7879, pp. 1–6, **2015**.

[15] J. McCollum, D. K. Smith, K. J. Hill, M. L. Pantoya, J. Warzywoda, N. Tamura, "A slice of an aluminum particle: Examining grains, strain and reactivity," *Combustion and Flame*, *vol. 173*, pp. 229–234, **2016**.

[16] V. I. Levitas, J. McCollum, M. L. Pantoya, N. Tamura, "Stress Relaxation in pre-stressed aluminum core-shell particles: X-ray diffraction study, modeling, and improved reactivity," *Combustion and Flame*, *vol. 170*, pp. 30–36, **2016**.

[17] V. I. Levitas, J. McCollum, M. L. Pantoya, N. Tamura, "Internal stresses in pre-stressed micron-scale aluminum core-shell particles and their Improved reactivity," *Journal of Applied Physics*, *vol. 118*, no. 9, pp. 094305, **2015**.

[18] M. Kuns, N. Tamura, K. Chen, A. A. MacDowell, R. S. Celestre, M. M. Church, S. Fakra, E. E. Domning, J. M. Glossinger, J. L. Kirschman, G. Y. Morrison, D. W. Plate, B. V. Smith, T. Warwick, V. V. Yashchuk, H. A. Padmore, E. Ustundag, "A dedicated superbend x-ray microdiffraction beamline for materials, geo-, and environmental sciences at the advanced light source," *AIP Review of Scientific Instruments*, *vol. 80*, no. 035108, **2009**.

[19] N. Tamura, "XMAS: A Veratile Tool for Analyzing Synchrotron X-ray Microdiffraction Data," in *Strain and Dislocation Gradients from Diffraction: Spacially-Resolved Local Structure and Defects*, Imperial College Press, pp. 125–155, **2014**.

[20] J. Hatch, Aluminum: Properties and Physical Metallurgy, Ohio, **1984**.

[21] H. Doore and H. Hubner, Alumina: Processing, Properties and Applications, Springer, Berlin, **2011**.

[22] J. A. Puszynski, C. J. Bulian and J. J. Swiatkiewicz, "Processing and Ignition Characteristics of Aluminum-Bismuth Trioxide Nanothermite System," *Journal of Propulsion and Power*, *vol. 23*, pp. 698–706, **2007**.

[23] D. A. Firmansyah, K. Sullivan, K.-S. Lee, Y. H. Kim, R. Zahaf, M. R. Zachariah, D. Lee, "Microstructural Behavior of the Alumina Shell and Aluminum Core Before and After Melting of Aluminum Nanoparticles," *J. Phys. Chem. C*, *vol. 116*, pp. 404–411, **2012**.

[24] V. I. Levitas, M. L. Pantoya, B. Dikici, "Melt dispersion versus diffusive oxidation mechanism for aluminum nanoparticles: Critical experiments and controlling parameters," *Applied Physics Letters*, *vol. 92*, no. 1, pp. 1–4, **2008**.

[25] S. Chaturvedi, P. N. Dave, "Solid propellants: AP/HTPB composite propellants," *Arabian Journal of Chemistry*, *vol. 12*, no. 8, pp. 2061–2068, **2015**.

[26] K. Sullivan, N. Piekiel, C. Wu, S. Chowdhury, S. Kelly, T. Hufnagel, K. Fezzaa, M. Zachariah, "Reactive Sintering: An Important component in the combustion of nanocomposite thermites," *Combustion and Flame*, *vol. 159*, pp. 2–15, **2012**.

[27] B. S. Bockman, M. L. Pantoya, S. F. Son, B. W. Asay and J. T. Mang, "Combustion velocities and propagation mechanisms of metastable interstitial composites," *Journal of Applied Physics*, *vol. 98*, no. 6, pp. 1–7, **2005**.

[28] J. J. Granier, M. L. Pantoya, "Laser ignition of nanocomposite thermites," *Combustion and Flame*, *vol. 138*, no. 4, pp. 373–383, **2004**.

[29] D. Krewski, R. A. Yokel, E. Nieboer, D. Borchelt, J. Cohen, J. Harry, S. Kacew, J. Lindsay, A. M. Mahfouz, V. Rondeau, "Human Health Risk Assessment for Aluminum, Aluminum Oxide, and Aluminum Hydroxide," *Journal of Toxicology and Environmental Health B*, *vol. 10*, no. 1, pp. 1–269, **2007**.

[30] V. I. Levitas, "Mechanochemical mechanism for reaction of aluminum nano- and micrometre-scale particles," *Phil Trans R Soc A*, *vol. 371*, no. 2003, **2013**.

[31] J. McCollum, M. L. Pantoya, S. T. Iacono, "Catalyzing aluminum particle reactivity with a fluorine oligomer surface coating for energy generating applications," *Journal of Fluorine Chemistry*, *vol. 180*, pp. 265–271, **2015**.

Manuscript received: September 5, 2020
Revised manuscript received: October 8, 2020
Version of record online: ■■, ■■■

FULL PAPER

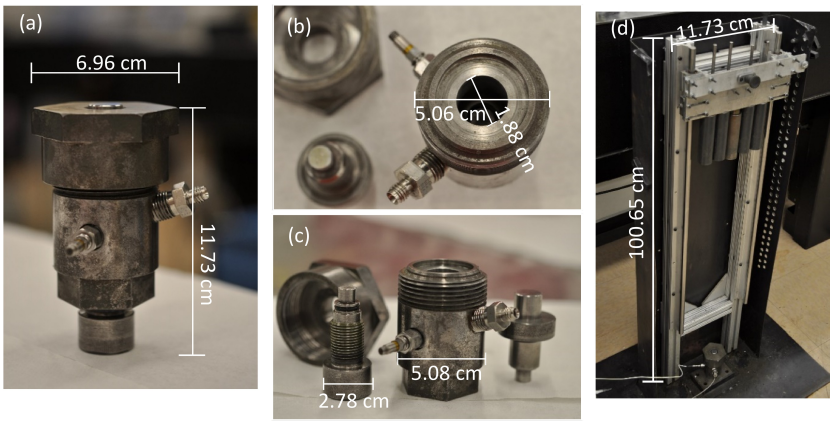

A. Williams, I. Shancita*, I. Altman*, N. Tamura*, M. L. Pantoya**